

# Niğde Ömer Halisdemir Üniversitesi Mühendislik Bilimleri Dergisi Niğde Ömer Halisdemir University Journal of Engineering Sciences

Araştırma makalesi / Research article





# Experimental investigation of wear behavior in Al<sub>2</sub>O<sub>3</sub>-reinforced glass fiber composites and comparative analysis of artificial neural network and machine learning models

Al<sub>2</sub>O<sub>3</sub> takviyeli cam elyaf kompozitlerde aşınma davranışının deneysel incelenmesi ve yapay sinir ağları ile makine öğrenmesi modellerinin karşılaştırmalı analizi

Rasit Koray Ergün<sup>1</sup>, İsmail Bayar<sup>2\*</sup>, Hüseyin Köse<sup>3</sup>

<sup>1, 2, 3</sup> Batman University, Department of Mechanical Engineering, 72100, Batman, Türkiye

#### **Abstract**

This study experimentally investigates the effects of adding different amounts (1-5 wt.%) of Al<sub>2</sub>O<sub>3</sub> particles on the wear behavior of glass fiber-reinforced epoxy composites to improve their tribological performance. Composite laminates produced using the hand-lay up method were subjected to wear tests using a ball-on-disc test setup under dry sliding conditions. Among all tested compositions, the composite containing 3 wt.% Al<sub>2</sub>O<sub>3</sub> exhibited the highest wear resistance. Compared to the neat composite, the specific wear rate was reduced by up to 70%. In contrast, 4% and 5% Al<sub>2</sub>O<sub>3</sub> additions resulted in a decrease in wear resistance due to particle agglomeration. While the highest specific wear rate was 260×10<sup>-6</sup> mm<sup>3</sup>/Nm, this value decreased to  $80 \times 10^{-6}$  mm<sup>3</sup>/Nm in the 3% added sample. Furthermore, wear rate predictions were performed using models such as artificial neural network and different machine learning regressors. Random Forest (17.62%), Ridge regressor (18.46) and artificial neural network (19.92%) achieved the lowest MAPE values, indicating strong predictive performance for Al<sub>2</sub>O<sub>3</sub>-reinforced glass fiber composites. The artificial neural network model optimized with grid search achieved a mean squared error of 0.90 and a coefficient of determination of 0.92, while the random forest regressor demonstrated strong generalization with a coefficient of determination of 0.91. The results demonstrated the critical roles of both particle ratio and data-driven models in wear performance analysis.

**Keywords:** GFRP, Wear, Al<sub>2</sub>O<sub>3</sub>, Machine learning, Artificial neural network

## 1 Introduction

Glass fiber reinforced polymer composites (GFRP) are widely used in many industries from aviation to automotive, from wind turbines to aircraft systems due to their advantages such as lightness, high mechanical strength, corrosion resistance and low cost [1]. Glass fibers show both thermal and chemical resistance because of their silica-based structures and increase the rigidity and impact resistance,

Öz

Bu çalışmada, cam elyaf takviyeli epoksi kompozitlerin tribolojik performanslarını iyileştirmek amacıyla farklı miktarlarda (%1-5 ağırlıkça) eklenen Al2O3 partiküllerinin asınma davranısları üzerindeki etkileri deneysel olarak araştırılmıştır. Elle yatırma yöntemiyle üretilen kompozit laminantlar, ball-on-disc bilye test düzeneği kullanılarak aşınma testlerine tabi tutulmuştur. Test edilen tüm numuneler arasında, %3 ağırlıkça Al2O3 içeren kompozit en yüksek aşınma direncini göstermiştir. Saf kompozitle karşılaştırıldığında, özgül aşınma oranı %70'e kadar azalmıştır. Buna karşılık, %4 ve %5 Al2O3 ilavesi, partikül aglomerasyonu nedeniyle aşınma direncinde bir azalmaya neden olmuştur. En yüksek özgül aşınma oranı 260x10-6 mm<sup>3</sup>/Nm iken, %3 eklenen numunede bu değer 80x10<sup>-6</sup> mm³/Nm'ye düşmüştür. Ayrıca, yapay sinir ağı ve farklı makine öğrenimi regresörleri kullanılarak asınma oranı tahminleri gerçekleştirilmiştir. En düsük değerlerine Random Forest (%17.62), Ridge regresörü (%18.46) ve ANN (%19.92) ulaşmış olup, bu da Al2O3 takviyeli cam elyaf kompozitler için güçlü tahmin performansına işaret etmektedir. Grid search metodu ile optimize edilen yapay sinir ağı modeli 0.9'lık bir ortalama karesel hata ve 0.92'lik bir belirlilik katsayısı değeri elde ederken, rastgele orman regresörü 0.91'lik bir belirlilik katsayısı değeriyle güçlü bir genelleme göstermiştir. Sonuçlar, aşınma performansı analizinde hem parçacık oranının hem de veri odaklı modellerin kritik rollerini ortaya koymuştur.

Anahtar kelimeler: GFRP, Aşınma, Al2O3, Makine öğrenmesi, Yapay sinir ağları

especially integrated with epoxy matrix systems [2]. In addition, glass fibers offer a more economical solution compared to high-performance fibers with their easy manufacturability and commercially affordable prices [3].

Composite structures are not limited to fiber reinforcement only but also hybridized with micro or nanosized ceramic particles, providing significant improvements in properties such as wear, hardness and high temperature

<sup>\*</sup> Sorumlu yazar / Corresponding author, e-posta / e-mail: ismailbyr@gmail.com (İ. Bayar) Geliş / Received: 28.07.2025 Kabul / Accepted: 25.09.2025 Yayımlanma / Published: 15.10.2025 doi: 10.28948/ngumuh.1752645

resistance [4]. In this context, aluminium oxide (Al<sub>2</sub>O<sub>3</sub>) stands out as an ideal particle reinforcement in glass fiber reinforced systems due to its improved hardness, chemical stability and heat transfer properties [5-8]. Load transfer efficiency was increased, and crack propagation is delayed by dispersing Al<sub>2</sub>O<sub>3</sub> particles in the polymer matrix. Furthermore, it provides significant surface hardness and improvements, which are tribological specifically advantageous for the parts exposed to corrosion [9]. Another aspect of the study is the prediction of wear behavior by processing experimental data with multiple regression models. The performance of the models under hyperparameters, both unoptimized and optimized with techniques such as grid search metod, was compared. This methodology offers an alternative to the time-consuming and costly nature of traditional wear tests, indicating that tribological behaviors can be predicted based on data-driven Artificial Intelligence - based models.

Glass fiber composite materials reinforced with alumina or other ceramic particles have been widely studied in tribological studies and data-driven prediction models. Sourabh K Singh et al. [10] developed an AI-based approach to predict the specific wear rates of glass fiber reinforced composites by adding different amounts of graphene nanoparticles into the epoxy matrix. In the study, R<sup>2</sup> scores of up to 99% were obtained using machine learning algorithms such as DNN, RF, GBM and XGBoost. The results revealed that parameters such as load and density have decisive effects on the wear behavior. Li et al. [11] investigated the effect of PTFE particle size on friction and wear properties in glass fiber reinforced epoxy matrix composites. Four different composites were produced with particle sizes ranging from 1 µm to 180 µm and it was observed that the lowest wear rate was obtained in the composites with the largest particle size. This was attributed to the fact that large particles increase the fiber anchoring effect and cause less deformation during wear. Similarly, in another study conducted by Kumar et al. [12] wear performances were evaluated using 0.5% and 1% graphene nanoparticles in glass fabric reinforced epoxy composites, and it was shown that specific wear rates could be successfully predicted with models developed with ANN, RF and GBM algorithms. This study emphasizes that strong correlations can be established between mechanical properties and tribological performance. Parikh and Gohil [13] evaluated the wear behavior under dry friction conditions by adding different amounts of graphite (3 and 5 wt%) to natural cotton fiber reinforced polyester composites. In the experiments carried out with Box-Behnken design, it was shown that graphite addition significantly increased the wear resistance, and the predictions made by ANN models were in high agreement with the experimental data. Padhi et al. [14] evaluated both mechanical and tribological properties of polypropylene matrix composites reinforced with short glass fibers by adding blast furnace slag (BFS). In the study conducted according to the Taguchi design, it was shown that the predictions generated by ANN models largely coincide with the experimental data and that the increase in the amount of BFS positively affects the wear resistance

(Padhi et al., Journal of Thermoplastic Composite Materials, 2015). Yadav et al. [15] systematically investigated the wear behavior of epoxy matrix composites by applying different ratios (0-20 wt%) of Al<sub>2</sub>O<sub>3</sub> and E-glass fiber reinforcement. In the experiments conducted with air jet erosion device, Taguchi L25 orthogonal array was used and reinforcement ratio, impact velocity, flow rate and impact angle were selected as the influencing factors. According to ANOVA analysis, it was determined that the impact velocity with 41% contribution ratio was the most determining factor on the wear rate. The lowest wear was obtained in the composite containing 10% Al<sub>2</sub>O<sub>3</sub>, at 30 m/s speed and 45° impact angle. SEM analyses revealed that Al<sub>2</sub>O<sub>3</sub> particles showed strong interfacial interaction with the matrix.

This study systematically investigates the effect of particle ratio on wear behavior by adding different ratios of Al<sub>2</sub>O<sub>3</sub> particles to glass fiber reinforced epoxy matrix composites that have an originally designed stacking sequence structure. Wear tests were performed at different load and distance parameters, and experimental results were evaluated based on specific wear rates and wear coefficients. SEM analyses were performed to understand surface morphologies, microstructural deteriorations and matrixparticle interfaces. In addition, wear losses were evaluated through the relationships established between the obtained general structural properties of the material and the applied experimental test parameters; these relationships were used in training artificial neural networks and machine learningbased algorithms, allowing the creation of predictive models. The simultaneous use of experimental wear characterization and machine learning-based predictive modeling constitutes a unique methodological contribution, offering a new perspective for correlating microstructural behavior with wear performance.

#### 2 Material and methods

### 2.1 Materials

In this study, glass fiber reinforced woven composite laminates were fabricated using the hand lay-up technique, which is one of the most common methods for manufacturing fiber-reinforced polymer matrix composites. Three types of glass fiber fabrics supplied by SPM Composite Company - SPM EGU 110 P (plain weave), SPM EGU 163 T (twill weave), and SPM EGU 195 T (weave structure) - were utilized as reinforcement materials. The fabrics possess areal densities of 110, 163, and 195 g/m², respectively, and corresponding fiber diameters of 9, 9, and 13  $\mu m$ . Prior to fabrication, all fabric sheets were cut into 100  $\times$  100 mm dimensions.

A resin system consisting of 80% ARC-152 epoxy resin and 20% W-152 hardener by volume was prepared and manually applied to each fabric layer to ensure adequate impregnation. A roller brush was employed to remove entrapped air and enhance interlaminar bonding. For additional reinforcement, approximately 98% pure  $Al_2O_3$  micro-particles (particle size: 0–50  $\mu$ m) were dispersed into the resin.

To investigate the effect of particle ratio on wear behavior, Al<sub>2</sub>O<sub>3</sub> particles were added by 1wt%, 2wt%, 3wt%, 4wt%, 5wt% ratios to glass fiber reinforced epoxy matrix composites. For the accuracy and repeatability of mechanical tests, homogeneous particle distribution within the epoxy matrix is crucial. To prevent agglomeration, the Al<sub>2</sub>O<sub>3</sub> particles were first stirred in a magnetic stirrer for 15 minutes and then dispersed in an ultrasonic bath for 60 minutes. The magnetic stirrer ensured even distribution of the particles within the resin, while the ultrasonic bath broke up particle clusters, resulting in a more homogeneous distribution. A symmetric six-layer composite laminate was constructed in the stacking sequence of [110P/163T/195T]s. The schematic representation of the stacking sequence is shown in Figure 1. Following lay-up, the laminates were cured at ambient conditions (~24 hours). The average thickness of the laminates was measured at three different points using a digital caliper, and found to be approximately 1.3 mm.

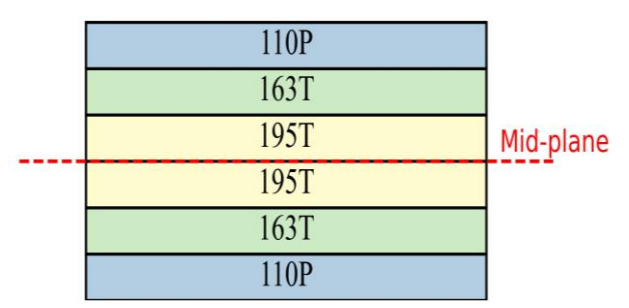


**Figure 1.** Schematic representation of the symmetric laminated composite structure with a [110P/163T/195T]s stacking sequence

#### 2.2 Wear test

Wear tests were conducted using a ball-on-disc configuration in accordance with ASTM G99 standards to evaluate the tribological performance of the composite laminates. AISI 304 stainless steel balls with a diameter of 6 mm were employed as the counterface material. Test samples were extracted from the central region of the composite plates. Wear tests were performed at room temperature (~23 °C) and 50% relative humidity under dry sliding conditions. The tests were conducted at a constant sliding speed of 3 cm/s, using two levels of normal load and

two different sliding distances. Each test was repeated three times to ensure reproducibility. The wear scar diameter was held constant at 6 mm throughout all trials. The specific wear rate was determined by measuring the volume loss due to wear and normalizing it with respect to the applied load and sliding distance. The design of experiment with the number of repetitions conducted under each condition is given in Table 1.

# 2.3 Artificial neural network and machine learning models

In this study, data-driven regression models were developed to predict the target variable using experimentally obtained wear loss. The modeling workflow was designed to include data preprocessing, algorithm implementation, performance evaluation, and systematic hyperparameter optimization. A total of 24 distinct composite configurations were fabricated as presented in Table 2. Considering that three independent tests were conducted for each configuration, the overall dataset size reached 72 experimental observations. In order to optimize the dataset, numerical variables were normalized using z-score standardization, and categorical variables were fitted to the model using one-hot encoding. These preprocessing steps aimed to minimize learning imbalances that could arise from inputs at different scales. The dataset was randomly split into training and testing subsets with an 80:20 ratio.

A wide range of regression models was employed to explore different learning behaviors and generalization capabilities. The models selected for this study included Artificial Neural Network (ANN), Decision Tree Regressor (DTR), Random Forest Regressor (RFR), Support Vector Regressor (SVR), K-Nearest Neighbor Regressor (KNNR), Extreme Gradient Boosting Regressor (XGBR), and Ridge Regressor (RR).

These models collectively represent both linear and non-linear learning paradigms, covering a wide spectrum of modeling techniques ranging from parametric to non-parametric, shallow to deep, and interpretable to complex. Each algorithm was chosen to capture distinct aspects of the data structure, such as feature interactions, local proximity patterns, kernel-based mappings, or deep nonlinear transformations.

No.	Al <sub>2</sub> O <sub>3</sub> (wt.%)	Force (N)	Distance (m)	No.	Al <sub>2</sub> O <sub>3</sub> (wt.%)	Force (N)	Distance (m)
1	Neat	7.5	150	13	%3	7.5	150
2	Neat	7.5	300	14	%3	7.5	300
3	Neat	15	150	15	%3	15	150
4	Neat	15	300	16	%3	15	300
5	%1	7.5	150	17	%4	7.5	150
6	%1	7.5	300	18	%4	7.5	300
7	%1	15	150	19	%4	15	150
8	%1	15	300	20	%4	15	300
9	%2	7.5	150	21	%5	7.5	150
10	%2	7.5	300	22	%5	7.5	300
11	%2	15	150	23	%5	15	150
12	%2	15	300	24	%5	15	300

A regression-based ANN model structured with an input layer and two hidden layers, each containing 32 and 16 neurons, respectively. ReLU was used as an activation function, and linear activation was used in the output layer. The model was optimized with Mean Squared Error (MSE) as the error function and updated using the Adam algorithm. 100 epochs were applied during the training process, and the model's early performance was monitored using a 10% validation set. Hyperparameters such as neuron numbers, learning rate, and batch size were comprehensively optimized using grid search strategy. The parameter combinations tested included the number of neurons in the hidden layers (16 and 32), activation functions (ReLU and tanh), optimization algorithms (Adam and SGD), and learning rates (0.001 and 0.01). A total of 64 different model configurations were trained, and the MSE performance for each model was calculated on the validation set. During this process, it was observed that the learning rate, optimizer selection, and activation functions played a critical role in the model's generalization ability. The final model was determined based on the configuration that provided the lowest MSE and the highest R2 value, as validated through k-fold cross-validation.

For the ML models, DTR was used with the default settings for parameters such as maximum depth and splitting criterion. RFR was run with an ensemble structure of 100 decision trees by default. SVR was implemented with RBF kernel function and default regularization parameter (C=1.0). KNNR was run using the number of neighbors k=5 and the Minkowski distance metric (p=2). XGBR was based on the library defaults of learning rate (0.1), maximum depth (6), and 100 trees. For RR, the L2 penalty was kept at the default α=1.0. Hyperparameter optimization for the ML models was performed using the grid search method. For the DTR, parameters such as maximum depth (3, 5, 10, None), split criteria (squared error, Friedman MSE), minimum number of leaves (1, 2, 4), and maximum feature selection (None, sqrt, log2) were scanned. For the RFR, the number of trees (50, 100, 200), maximum depth (None, 5, 10, 20), minimum sample split (2, 5, 10), minimum number of leaves (1, 2, 4), and maximum feature selection (auto, sqrt, log2) were evaluated. For SVR, different kernel functions (linear, rbf, poly, sigmoid), regularization parameter C (0.1–1000), epsilon (0.001-1.0), gamma (scale, auto, fixed values) and degree (2-5) for the polynomial kernel have been extensively tested. For KNNR, the number of neighbors (1 to 29), weighting functions (uniform, distance), distance metrics (euclidean, manhattan, minkowski), p parameter (1, 2) and algorithm selection (auto, ball tree, kd tree, brute) have been investigated. For RR, the regularization coefficient α (in the range of 10<sup>-4</sup>-10<sup>3</sup>), solution algorithms (auto, svd, cholesky, lsqr, sparse cg, sag, saga) and inclusion or exclusion of the intercept term have been optimized. With these comprehensive parameter scanning, the performance of each algorithm was systematically evaluated multidimensional hyperparameter space, and the models that provided the lowest mean squared error (MSE) were used to obtain the final results.

Absolute Percentage Error (APE) and Mean Absolute Percentage Error (MAPE) metrics were also used to evaluate the predictive performance of the predictive models by using Equations 1 and 2. APE provides a percentage difference between the predicted and actual values for each test dataset which demonstrates the model's performance on individual samples. MAPE provides an assessment of the overall predictive power of the models by presenting the average error rate calculated across all test samples. Using these two together metrics allows for comparison of both sample-by-sample deviations and overall performance.

$$APE = \left| \frac{y_i - \widehat{y}_l}{v_i} \right| x100\%$$

MAPE = 
$$\frac{100\%}{n} \sum_{i=1}^{n} \left| \frac{y_i - \hat{y}_i}{y_i} \right|$$
 2

Mean Squared Error (MSE) and the coefficient of determination (R²) were employed by using the equations 3 and 4 as standard regression metrics, providing complementary insights into the absolute error magnitude and the proportion of variance explained by the models. The combined use of APE, MAPE, MSE, and R² ensures a comprehensive evaluation of model accuracy and generalization capability.

$$MSE = \frac{1}{n} \sum_{i=1}^{n} (y_i - \hat{y}_i)^2$$
 3

$$R^{2} = 1 - \frac{\sum_{i=1}^{n} (y_{i} - \hat{y}_{i})^{2}}{\sum_{i=1}^{n} (y_{i} - \bar{y})^{2}}$$
 4

# 3 Results and discussion

# 3.1 Wear behavior

The results of the wear tests were evaluated based on the analysis of average mass loss, specific wear rate, friction coefficient, and scanning electron microscopy (SEM) images of the worn surfaces. The tests were performed under two loads (7.5 N and 15 N) and over two sliding distances (150 m and 300 m). Figure 2 presents the average mass loss of GFRP composites containing Al<sub>2</sub>O<sub>3</sub> powder in various proportions (1-5%), tested under four distinct wear conditions. Neat samples exhibited the highest wear values, specifically observing a mass loss of approximately 13.8 mg under a load of 15 N and a distance of 300 m. In contrast, the mass loss in the sample obtained with 3% Al<sub>2</sub>O<sub>3</sub> added under the same test conditions decreased to approximately 6.8 mg, indicating an improvement of over 50%. Similarly, at a load of 7.5 N and 150 m, the mass loss of the neat sample was approximately 5.1 mg, whereas this value decreased to 1.6 mg in the composite with 3% Al<sub>2</sub>O<sub>3</sub>, corresponding to a reduction of about 69%.

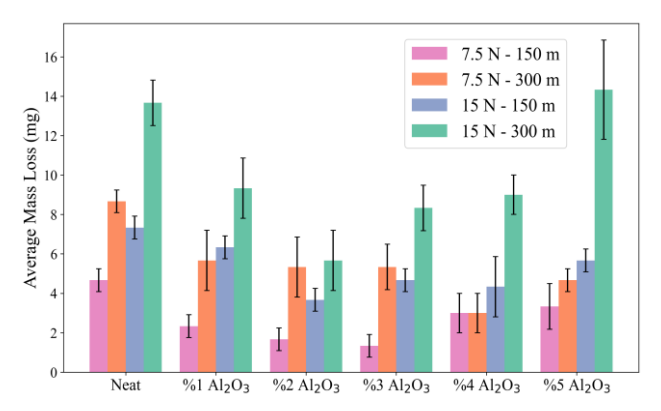


Figure 2. Average mass loss of the samples

A similar decrease in wear loss was observed when the Al<sub>2</sub>O<sub>3</sub> content was increased to 1% and 2%, but this improvement was more limited compared to the 3% Al<sub>2</sub>O<sub>3</sub> content. For example, while the loss in the neat sample at 15 N and 150 m was 8.2 mg, this value decreased to 4.7 mg in the 2% Al<sub>2</sub>O<sub>3</sub> sample, representing an approximately 43% improvement. In contrast, increasing the Al<sub>2</sub>O<sub>3</sub> content to 4% and 5% resulted in a significant decrease in wear resistance. Notably, the composites with 5% Al<sub>2</sub>O<sub>3</sub> exhibited wear performance similar to or even worse than the neat sample under certain conditions. This suggests microstructural problems such as the inhomogeneous dispersion of high powder content within the matrix, increased particle agglomeration, and the formation of localized weakness zones

Overall, the composite with 3% Al<sub>2</sub>O<sub>3</sub> additive exhibited optimal performance across all tested conditions, reducing mass loss by 40% to 70% compared to the neat composite. This significant reduction in wear rate reveals the load-carrying capacity of the Al<sub>2</sub>O<sub>3</sub> particles within the composite structure and their ability to prevent microwear, while clearly demonstrating that increasing the Al<sub>2</sub>O<sub>3</sub> content ( $\geq 4\%$ ) can negatively impact wear performance. The findings of this study are consistent with similar studied in the literature. Optimum nanoparticle addition, particularly in the 2–5% range, significantly improves the tribological properties of epoxy-based composites, but higher addition rates cause performance degradation due to particle agglomeration [16, 17].

Figure 3 shows the specific wear rates of the composites. The general trend indicates that the addition of Al<sub>2</sub>O<sub>3</sub> significantly reduces the specific wear rate. The specific wear rate of the neat composite is highest, approximately 260x10<sup>-6</sup> mm<sup>3</sup>/Nm at a load of 7.5 N and a distance of 150 m. In contrast, the 3% Al<sub>2</sub>O<sub>3</sub>sample under the same conditions exhibits a specific wear rate of approximately 80x10<sup>-6</sup> mm<sup>3</sup>/Nm, which corresponds to a reduction of approximately 69%. Wear rates of all composites varied with applied load and sliding distance. For example, the specific wear rate for the neat composite at 15 N and 300 m was approximately 160x10<sup>-6</sup> mm<sup>3</sup>/Nm, which decreased to 110x10<sup>-6</sup> mm<sup>3</sup>/Nm for the composite with 3% Al<sub>2</sub>O<sub>3</sub>. Similarly, the specific wear rates for the composites containing 1% and 2% Al<sub>2</sub>O<sub>3</sub> decreased compared to the neat

composite. Specifically, with the 2% Al<sub>2</sub>O<sub>3</sub> addition, the specific wear rate at 15 N and 300 m was approximately 90x10<sup>-6</sup> mm<sup>3</sup>/Nm, corresponding to an improvement of about 44% compared to the neat sample. However, at additive ratios of 4% and 5%, a similar trend in specific wear rates is observed as in the mass loss results. In particular, the composite containing 5% Al<sub>2</sub>O<sub>3</sub> exhibited a specific wear rate of approximately 170x10<sup>-6</sup> mm<sup>3</sup>/Nm under the 15 N and 300 m condition, corresponding to about 55% lower wear resistance than the composite with 3% Al<sub>2</sub>O<sub>3</sub>. This finding suggests that high additive ratios negatively affect specific wear resistance by causing particle agglomeration and matrix-phase weakening in the microstructure.

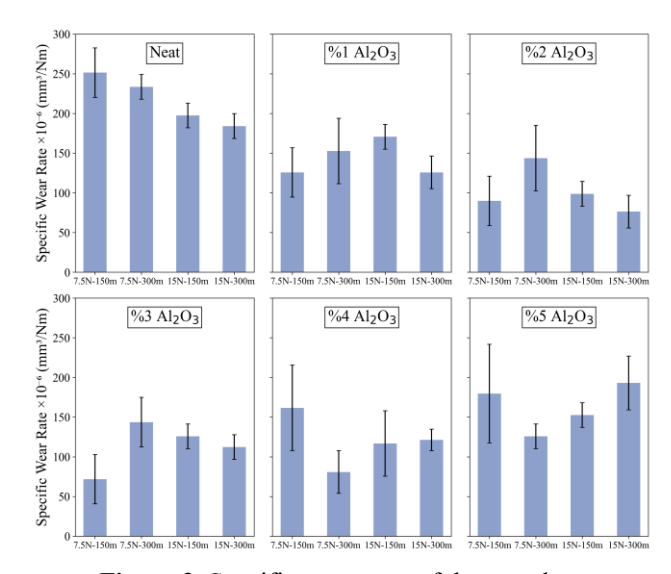


Figure 3. Specific wear rates of the samples

SEM images of the worn surfaces of the neat composite and the composite containing 3%  $Al_2O_3$  are presented in Figure 4. The neat sample exhibited relatively large worn surface (~1504  $\mu$ m), prominent plucked fiber regions, and widespread wear debris, indicating poor fiber–matrix interfacial bonding and mechanical separation.

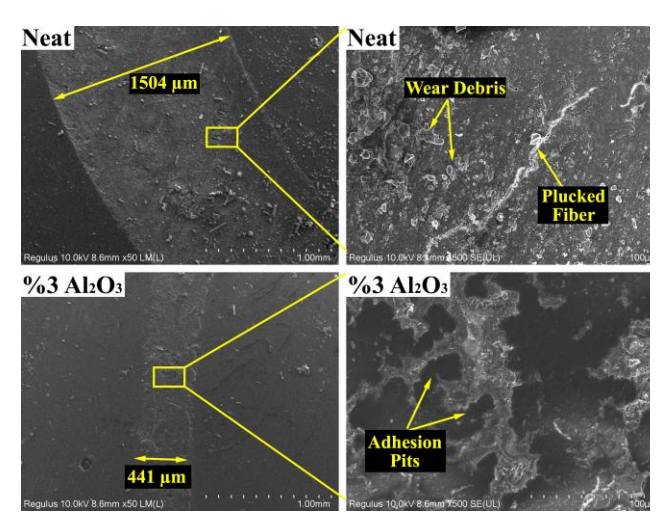


Figure 4. SEM images of worn surfaces

In contrast, the worn surface in the 3% Al<sub>2</sub>O<sub>3</sub>-reinforced composite is significantly smaller (~441 µm), the wear surface becomes smoother, and only isolated adhesion pits are observed. This microstructural improvement is directly related to the minimal mass loss and low specific wear rate observed at the 3% Al<sub>2</sub>O<sub>3</sub> containing composite. The Al<sub>2</sub>O<sub>3</sub> particles act as a protective barrier on the surface, inhibiting fiber-matrix separation and microcrack propagation.

Figure 5 illustrates the variation in the coefficient of friction ( $\mu$ ) of the composite materials as a function of the applied load and the sliding distance. Under all test conditions, the coefficient of friction exhibits a characteristic increase at the beginning of the test (the first ~10–30 m) and then reaches a relatively stable regime.

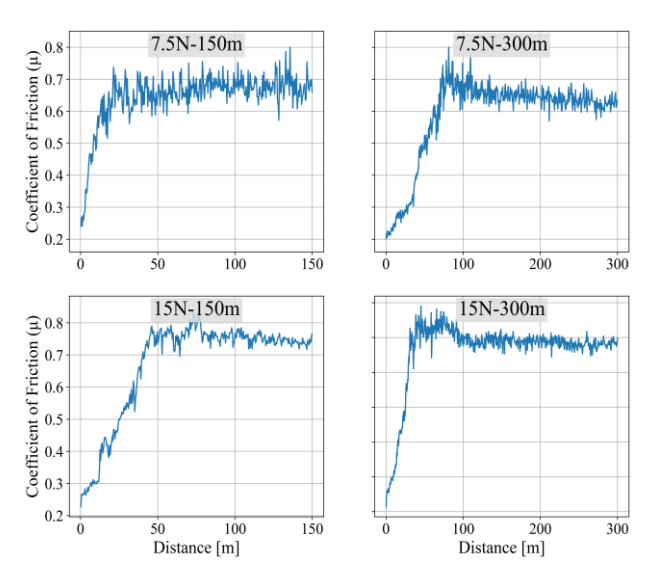


Figure 5. The COF of the samples

Increasing the applied load resulted in a significant rise in the coefficient of friction (COF); while COF remained nearly constant at approximately 0.65 under a 7.5 N load, it increased to 0.75-0.80 at a 15 N load. This increase indicates that microscopic deformations and plastic yielding at the contact surface intensified. As the sliding distance increased to 300 m, the fluctuations in the COF decreased, and the system entered a more stable regime, indicating that the surface had reached tribological equilibrium and the influence of wear debris had diminished. Thus, although higher loads increased friction, extended sliding distances contributed to friction stabilization.

# 3.2 Comparative analysis of data-driven predictive modeling approaches

In this study, an artificial neural network (ANN) model was implemented to evaluate the predictive capability of the proposed approach, and its training behavior is presented in detail. Figure 6 visually presents the training process and prediction performance of the ANN model.

The loss plot of the ANN model shows that both training and validation errors are decreasing steadily, and the model is able to learn without overfitting. In the prediction performance plot, the predictions are generally distributed close to the perfect fit line; this shows that the model works

with high accuracy on the training data and achieves a strong fit, especially in the middle value range. Although there are small deviations in the extreme values, the overall prediction performance is satisfactory.

In addition to ANN, different machine learning models were also used for comparison purposes in this study and their results were analyzed comparatively. In this context, Decision Tree Regressor (DTR), Random Forest Regressor (RFR), K-nearest Neighbor Regressor (KNNR), Support Vector Regressor (SVR), XGBoost Regressor (XGBR), Ridge Regressor (RR) and Lasso Regressor (LR) were used, but due to the weak results obtained in the preliminary studies, Lasso was removed from the analysis. The scatter plot graphics of the training data presented in Figure 7 show the degree to which the values predicted by each model overlap with the actual values.

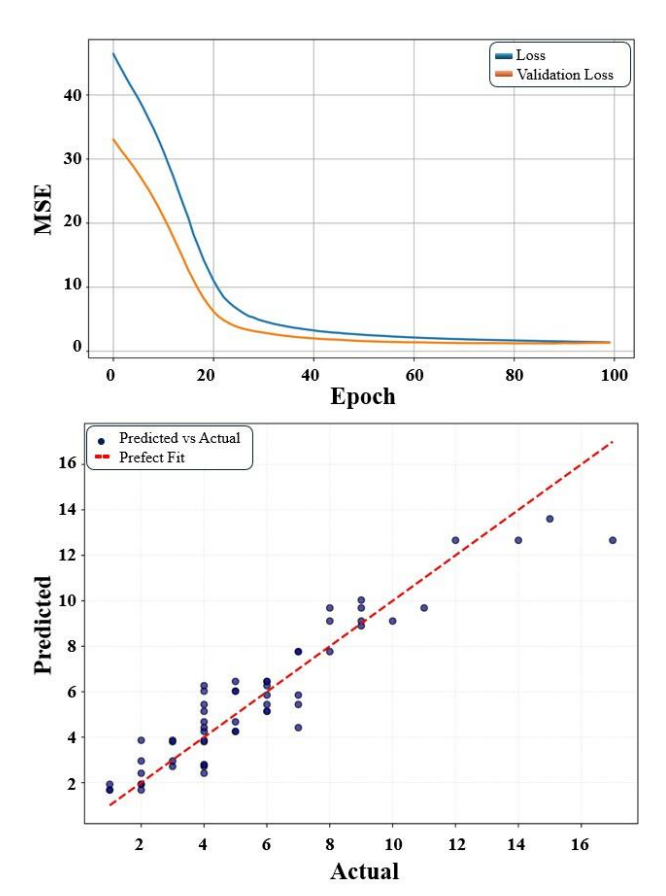


**Figure 6.** The loss and prediction performance of the ANN model

The RFR and XGBR models exhibited strong learning performance based on the perfect fit line. The RR model also shows a fairly balanced distribution, providing high fit especially in the middle range. Although Support SVR and DTR models have caught the general trend, some deviations are noticeable. The weakest distribution is observed in the KNNR model; especially in the middle and high value ranges, the points move away from the perfect fit line, indicating overly simplistic generalization. In general, RFR, XGBR and RR models gave the most successful results on the training data.

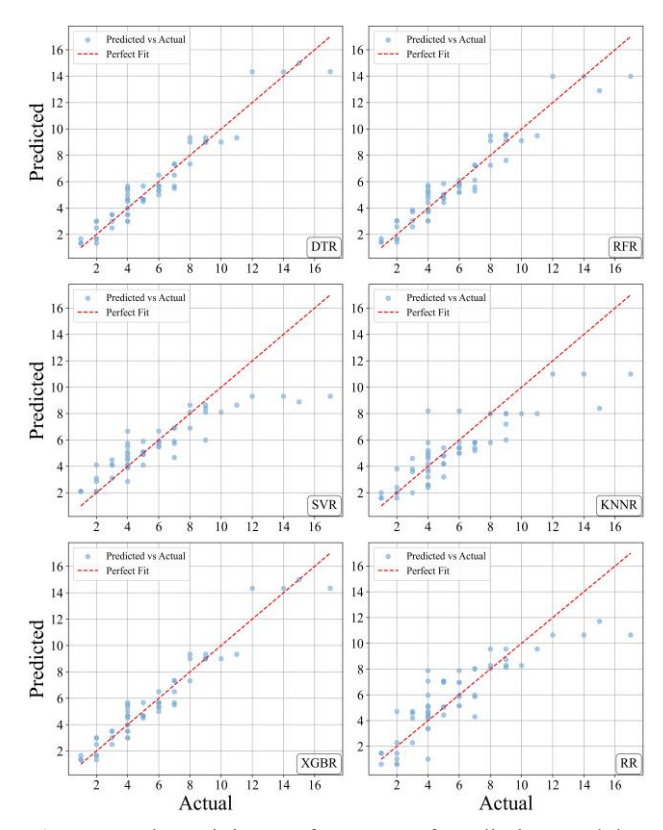


Figure 7. The training performance of predictive models

Figure 7 indicates that the RFR and RR models stand out with their estimation curves being close to the actual values, especially the RFR model shows high generalization success in the medium and high index range. The RR model provided stable and low-deviation results in linear data. Although the XGBR model caught the general trend, it increased the error rate with significant deviations in high range samples. DTR produced successful predictions at most points, but sudden deviations were observed in extreme values. SVR follows the general trend but is particularly indecisive in high range values. The KNNR model is the model that deviates the most from the actual values and has experienced a significant loss of accuracy, especially in the medium and large value range. This analysis reveals that the RFR and RR models have strong generalization ability on this data set, while KNNR and SVR are sensitive to parameters and require strong parameter optimization.

Table 2 compares the predicted values obtained from different machine learning models for each test data set with the actual values and calculates the absolute percentage error (APE). This provides a detailed overview of the predictive performance of the models based on the input parameters.

The APE values calculated for each test dataset reveal the sensitivity of the models to experimental conditions. Especially under low load (7.5 N) and short sliding distance (150 m), the actual wear values are quite small, and although the error rates are limited in absolute terms, the APE percentage increases. This suggests that small wear values are more sensitive to the normalized error percentage. The Table 2 results reveal that the ANN and RFR models can maintain APE values below 10% in most scenarios, whereas

SVR and some tree-based methods can produce deviations in the range of 40–100% under certain conditions. Furthermore, it was observed that model predictions differed with increasing Al<sub>2</sub>O<sub>3</sub> addition ratio; ANN and RFR were more stable at low addition levels (1–2%), while some models' generalization ability decreased at higher addition levels. These findings highlight the relative importance of input variables on wear behavior and suggest that model accuracy should be carefully evaluated, especially with small-scale experimental data.

Figure 8 presents a comparison of the mean absolute percentage error (MAPE) values calculated across all test data. This display allows us to compare the overall predictive success of each model across the entire dataset and to visualize the performance differences between models.

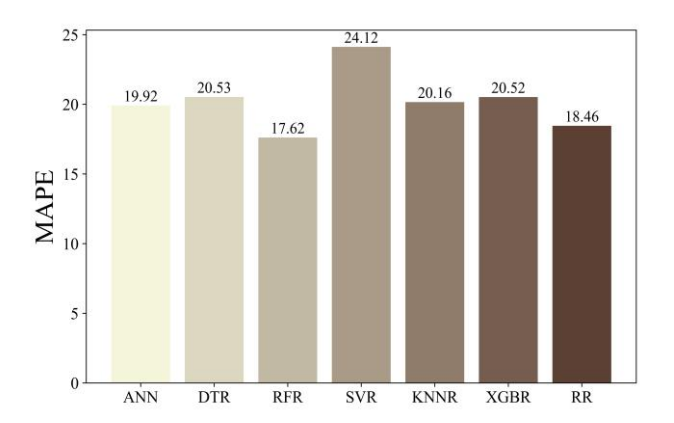


Figure 8. MAPE of the predictive models

The MAPE values presented in Figure 8 demonstrate that the lowest error rate was achieved with the RFR model at 17.62%, indicating that the combination of ensemble-based random sampling and multiple decision trees improves generalization ability in noisy and limited-dimensional datasets. RR provided a similarly low error rate of 18.46%, while the ANN model demonstrated acceptable accuracy at 19.92%. In contrast, SVR model reached the highest error rate of 24.12%, suggesting that nonlinear kernel-based methods fail to achieve optimal parameter fitting on the current dataset. KNNR, DTR, and XGBR showed moderate performance with error rates in the range of 20–21%. The general trend indicates that ensemble methods and regularization-based linear models provide more reliable results, while the ANN maintains reasonable error levels despite different parameter combinations. These evaluations clearly reveal that both the size and distribution of the data set and the parametric structure of the model should be taken into account in model selection.

Mean Squared Error (MSE) and Coefficient of Determination  $(R^2)$  values obtained by different regression algorithms on test data with non-optimized parameters are shown in Figure 9.

APE (%) 69.15 11.25 14.03 66.13 12.58 14.44 23.36 24.77 2.15 966 4.88 9.75 2.96 966 RR Pred. 8.12 4.44 4.30 11.71 7.88 4.60 8.73 4.20 11.71 8.73 8.12 5.87 1.02 28.56 25.00 41.66 12.49 28.56 76'66 15.37 15.37 APE (%) 8.32 66.6 86.6 0.02 0.00 0.01 15.00 15.00 Pred. 9.00 4.00 6.50 4.50 5.50 3.00 5.00 2.50 3.50 9.00 3.50 9.00 9.00 30.00 10.00 36.00 20.00 35.38 17.14 23.33 20.00 10.00 35.38 33.33 APE (%) 4.00 0.00 Pred. 4.6 3.2 2.6 5.4 5.2 2.4 8.4 8.2 7.2 3.6 8.4 7.7 9 9 N 33.43 25.11 95.00 55.00 25.23 APE (%) 18.01 31.61 31.61 19.87 4.60 2.50 1.67 6.57 6.77 SVR Pred. 4.10 3.10 4.10 5.99 3.90 4.67 2.86 8.89 4.49 8.89 8.39 5.99 5.90 6.67 8.39 11.48 18.18 29.35 36.73 15.36 35.66 APE (%) 89.21 0.73 1.83 6.05 0.71 6.34 0.73 RFR 12.90 12.90 Pred. 7.62 3.78 6.11 4.43 5.30 3.02 5.73 2.59 3.86 9.57 9.57 7.62 3.71 12.50 15.38 25.00 15.38 10.00 10.00 28.57 41.67 12.50 28.57 APE (%) 8.33 0.00 0.00 0.00 100 DIR Pred. 6.5 4.5 5.5 2.5 3.5 3.5 15 5 15 6 6 0 d 3 0 64.55 15.33 38.03 25.87 42.09 38.57 APE (%) 4.87 2.87 4.86 10.51 14.7 9.91 9.6 9.91 ANN Table 2 APE analysis of the predictive models 14.28 14.28 Pred. 5.70 5.14 2.55 5.92 3.29 8.56 2.96 9.94 2.77 3.71 9.94 4.51 Actual Val. 13 13 N 9 10 0 N 9 0 4 -6 Distance (m) 300 150 150 300 150 150 300 300 150 150 300 150 300 300 300 Force (N) 7.5 7.5 7.5 7.5 7.5 7.5 7.5 15 12 15 15 15 15 15 15 Sample Neat Neat Neat Neat Neat 1% 2% 84 2% 5% 9%4 %2 6%3 6%3 %1



**Figure 9.** Obtained MSE and  $R^2$  values for the predictive models

Initial findings from the evaluation of non-optimized models have shown that especially RFR and ANN models with provide high accuracy even hyperparameters. While RFR model stands out with 1.28 MSE and 0.88 R<sup>2</sup> score, ANN showed a similarly satisfactory performance with 1.41 MSE and 0.87 R<sup>2</sup> value. Similarly, RR also provided high initial accuracy with 1.11 MSE and 0.890 R<sup>2</sup> score when trained with default inputs for solver. In this context, it has been seen that algorithms with relatively low parametric sensitivity and robust behavior even under default configurations can be the first choice for small data sets or rapid prototyping processes. However, the fact that some models (especially SVR and KNNR) show very low performance with default settings emphasizes the importance of hyperparameter tuning.

The SVR and KNNR models in the graph showed significantly lower performance compared to other methods. In particular, KNNR draws attention with a relatively high MSE value of 4.43 compared to other models, while only showing a poor performance to explain the data variance with an R² score of 0.59. Similarly, the SVR model exhibited a low overall fit with a MSE of 3.82 and an R² value of 0.64. This can be attributed to the fact that both models have high parameter sensitivity and the accuracy level decreases dramatically with unoptimized parameters. Inappropriate selection of kernel, C and epsilon values in SVR; inappropriate adjustment of the k-neighborhood number and distance metric in KNNR may have directly affected the model success.

Grid search method was used to optimize hyperparameters in all predictive models. The graph presented in Figure 10 shows the MSE and  $R^2$  values obtained after determining the optimal hyperparameters of each model with the grid search method.

After hyperparameter optimization, the best performance was achieved with the Artificial Neural Network (ANN) model. The final architecture consisted of a first hidden layer with 32 neurons using the *tanh* activation function and a second hidden layer with 32 neurons using the ReLU activation function. The network was trained with the Adam optimization algorithm and a learning rate of 0.001.

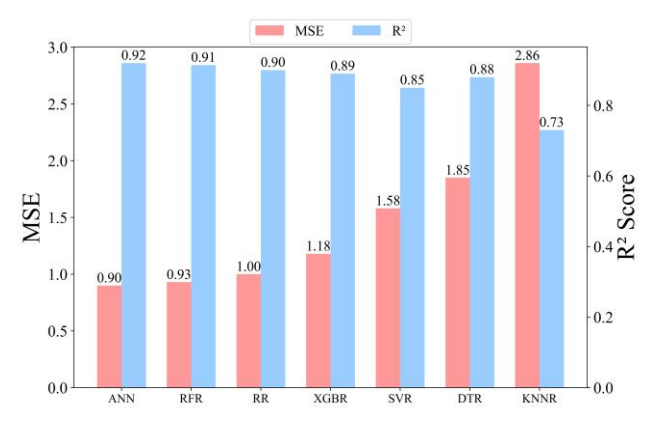


**Figure 10.** Obtained MSE and  $R^2$  values for the predictive models after hyperparameter optimization

This configuration yielded the lowest MSE (0.90) and the highest R<sup>2</sup> (0.92). The Random Forest Regressor (RFR), with unlimited depth, log2-based feature selection, and optimized sample split values, achieved an MSE of 0.93 and an R<sup>2</sup> of 0.91, confirming the strong generalization ability of the ensemble approach. For Ridge regression, the optimal structure was obtained with a regularization parameter  $\alpha = 0.1$  and solver = saga, resulting in an MSE of 1.00 and an R<sup>2</sup> of 0.90. In contrast, SVR, optimized with parameters C = 0.1,  $\epsilon = 0.1$ , polynomial kernel (degree = 3), and  $\gamma = \text{scale}$ , produced an MSE of 3.19 with limited predictive capacity. Similarly, the K-Nearest Neighbors Regressor (KNNR), with algorithm selection, leaf size = 40, and Minkowski distance metric (p = 2), achieved an MSE of 2.87 and an R<sup>2</sup> of 0.74

These results demonstrate that ANN and RFR models stand out with their high accuracy and generalization capacity, Ridge regression provides a competitive performance with simpler structure, while SVR and KNNR exhibit relatively lower accuracy depending on the data structure and parameter sensitivity. Similar findings have been reported in the literature, where nanofiller-reinforced composites combined with advanced ML models such as RFR, gradient boosting, and deep neural networks have demonstrated high predictive accuracy with R<sup>2</sup> values frequently above 0.90 [18-20].

On the other hand, the effect of optimization is much more striking for SVR and KNNR models. The SVR model, which has a default MSE value of 3.82, has achieved a 59% reduction in error by reaching 1.58 MSE in its optimized state and has increased the R² score from 0.64 to 0.85. Similarly, the KNNR model has shown a significant increase in accuracy by increasing from 4.43 MSE and 0.59 R² to 2.86 MSE and 0.73 R². These results clearly show that the parameter sensitivity of such models is very high and that they are unlikely to produce meaningful results unless they are optimized.

When evaluated specifically for DTR, an interesting finding is that the model did not provide a significant increase in R<sup>2</sup> score despite optimization. While the MSE value slightly decreased from 1.90 to 1.85, the R<sup>2</sup> score increased from 0.82 to 0.88. This limited improvement may be due to the over-learning nature of decision trees and

indicates that such models may have low generalization capacity, especially in limited sample sizes.

As a result, the analysis performed showed the positive effect of parameter optimization on model success in all models. However, the magnitude of this effect varies depending on the model and is more pronounced in algorithms with high parametric sensitivity such as SVR and KNNR. Systematic and careful implementation of hyperparameter search processes not only increases the generalization ability of the model but can also reduce the error by more than half in some cases.

#### 4 Conclusions

In this study, Al<sub>2</sub>O<sub>3</sub> microparticle reinforcement was applied at different ratios (1-5 wt.%) to improve the wear behavior of glass fiber-reinforced epoxy composites, and the tribological performance of the resulting composites was investigated. Furthermore, the obtained experimental data were analyzed using an artificial neural network and various machine learning algorithms to estimate specific wear rates.

- The addition of Al<sub>2</sub>O<sub>3</sub> particles enhanced the tribological performance of glass fiber-reinforced epoxy composites. Notably, the composite with 3 wt.% Al<sub>2</sub>O<sub>3</sub> exhibited the lowest specific wear rate, achieving a 69% reduction in mass loss and an approximate 70% decrease in specific wear rate compared to the neat composite.
- At 4 5 wt.% Al<sub>2</sub>O<sub>3</sub> content, particle agglomeration led to microstructural deterioration, which in turn resulted in reduced wear resistance.
- As part of the data-driven modeling, Artificial Neural Network (ANN), Random Forest Regressor (RFR), Ridge Regressor, Support Vector Regressor (SVR), and other regression algorithms were evaluated, and hyperparameter optimization was performed using the GridSearch method. The optimized ANN model achieved the highest accuracy with an MSE of 0.90 and an R<sup>2</sup> of 0.92, while the RFR model demonstrated strong generalization ability with an R<sup>2</sup> score of 0.91.
- The analyses showed that the wear resistance of Al<sub>2</sub>O<sub>3</sub> doped glass fiber composites can be successfully predicted using machine learning models. Sample-based APE values indicate that prediction errors increase, particularly under low-load and short-distance conditions, but that ANN and RFR generally provide more stable results. In terms of the average error metric MAPE, the RFR model had the lowest error rate of 17.62%, followed by RR at 18.46% and ANN at 19.92%. In contrast, the SVR model had the highest error rate of 24.12%. These findings demonstrate that the RFR and RR models, in particular, offer more reliable methods for predicting the wear behavior of doped composites.
- Models such as SVR and KNNR achieved error reductions of 59% and 35%, respectively, after optimization. These results demonstrate that properly configured AI models offer an effective alternative for tribological property prediction.

# **Conflict of interest**

The author declares that there is no conflict of interest.

#### Similarity rate (iThenticate): %12

#### References

- [1] P. K. Mallick, Fiber-Reinforced Composites: Materials, Manufacturing, and Design, Third Edition. 2007. https://doi.org/10.1201/9781420005981.
- [2] Z. Cao, T. Hao, P. Wang, Y. Zhang, B. Cheng, T. Yuan, and J. Meng, Surface modified glass fiber membranes with superior chemical and thermal resistance for O/W separation. Chemical Engineering Journal, 309, 30-40, 2017. https://doi.org/10.1016/j.cej.2016.10.013.
- [3] A. Kumre, R. S. Rana, and R. Purohit, A Review on mechanical property of sisal glass fiber reinforced polymer composites. Materials Today: Proceedings, 4, 2, Part A, 3466-3476, 2017. https://doi.org/10.1016/ j.matpr.2017.02.236.
- [4] A. C. Detomi, R. M. D. Santos, S. L. M. R. Filho, C. C. Martuscelli, T. H. Panzera, and F. Scarpa, Statistical effects of using ceramic particles in glass fibre reinforced composites. Materials & Design, 55, 463-470, 2014. https://doi.org/10.1016/j.matdes.2013.09.026.
- [5] A. Mohanty, V. K. Srivastava, and P. U. Sastry, Investigation of mechanical properties of alumina nanoparticle-loaded hybrid glass/carbon-fiberreinforced epoxy composites. Journal of Applied Polymer Science, 131, 1, 2014. https://doi.org/10.1002/ app.39749.
- [6] S. A. B. Lins, M. C. G. Rocha, and J. R. M. d'Almeida, Mechanical and thermal properties of high-density polyethylene/alumina/glass fiber hybrid composites. Journal of Thermoplastic Composite Materials, 32, 11, 1566-1581, 2019. https://doi.org/10.1177/0892705718 797391.
- [7] A. Fathy, A. Shaker, M. A. Hamid, and A. Megahed, The effects of nano-silica/nano-alumina on fatigue behavior of glass fiber-reinforced epoxy composites. Journal of Composite Materials, 51, 12, 1667-1679, 2017. https://doi.org/10.1177/0021998316661870.
- [8] A. Mohanty and V. K. Srivastava, Effect of alumina nanoparticles on the enhancement of impact and flexural properties of the short glass/carbon fiber reinforced epoxy based composites. Fibers and Polymers, 16, 1, 188-195, 2015. https://doi.org/ 10.1007/s12221-015-0188-5.
- [9] M. Abu-Okail, N. A. Alsaleh, W. M. Farouk, A. Elsheikh, A. Abu-Oqail, Y. A. Abdelraouf, and M. A. Ghafaar, Effect of dispersion of alumina nanoparticles and graphene nanoplatelets on microstructural and mechanical characteristics of hybrid carbon/glass fibers reinforced polymer composite. Journal of Materials Research and Technology, 14, 2624-2637, 2021. https://doi.org/10.1016/j.jmrt.2021.07.158.
- [10] K. Sourabh K Singh, S. Kumar, and K. K. Singh, Computational data-driven based optimization of tribological performance of graphene filled glass fiber reinforced polymer composite using machine learning approach. Materials Today: Proceedings, 66, 3838-

- 3846, 2022. https://doi.org/10.1016/ j.matpr.2022.06 .253.
- [11] Z. Li, X. Qi, C. Liu, B. Fan, and X. Yang, Particle size effect of PTFE on friction and wear properties of glass fiber reinforced epoxy resin composites. Wear, 532-533, 205104, 2023. https://doi.org/10.1016/j.wear.2023.205104.
- [12] S. Kumar, K. S. K. Singh, and K. K. Singh, Data-driven modeling for predicting tribo-performance of graphene-incorporated glass-fabric reinforced epoxy composites using machine learning algorithms. Polymer Composites, 43, 9, 6599-6610, 2022. https://doi.org/10.1002/pc.26974.
- [13] H. H. Parikh and P. P. Gohil, Experimental investigation and prediction of wear behavior of cotton fiber polyester composites. Friction, 5, 2, 183-193, 2017. https://doi.org/10.1007/s40544-017-0145-y.
- [14] P. K. Padhi, A. Satapathy, and A. M. Nakka, Processing, characterization, and wear analysis of short glass fiber-reinforced polypropylene composites filled with blast furnace slag. Journal of Thermoplastic Composite Materials, 28, 5, 656-671, 2015. https://doi.org/10.117 7/0892705713486142.
- [15] R. Yadav, H.-H. Lee, A. Meena, and Y. K. Sharma, Effect of alumina particulate and E-glass fiber reinforced epoxy composite on erosion wear behavior using Taguchi orthogonal array. Tribology International, 175, 107860, 2022. https://doi.org/10.1016/j.triboint.2022.107860.
- [16] K. P. Srinivasa Perumal, L. Selvarajan, K. P. Manikandan, and C. Velmurugan, Mechanical, tribological, and surface morphological studies on the

- effects of hybrid ilmenite and silicon dioxide fillers on glass fibre reinforced epoxy composites. Journal of the Mechanical Behavior of Biomedical Materials, 146, 106095, 2023. https://doi.org/10.1016/ j.jmbbm. 2023.106095.
- [17] P. Singh, S. Singh, R. Ojha, P. Tiwari, S. Khan, R. Kumar, and A. Gupta, Characterization of wear of FRP composites: A review. Materials Today: Proceedings, 64, 1357-1361, 2022. https://doi.org/10.1016/j.matpr.2022.04.236.
- [18] K. A. Sheikh and M. M. Khan, Predictive modeling of abrasive wear in in-situ TiC reinforced ZA37 alloy: A machine learning approach. Tribology International, 202, 110291, 2025. https://doi.org/10.1016/ j.triboint.2024.110291.
- [19] M. D. Kiran, L. Y. B R, A. Babbar, R. Kumar, S. C. H S, R. P. Shetty, S. K B, S.K. L, R. Kaur, M. Q. Alkahtani, S. Islam, and R. Kumar, Tribological properties of CNT-filled epoxy-carbon fabric composites: Optimization and modelling by machine learning. Journal of Materials Research and Technology, 28, 2582-2601, 2024. https://doi.org/10.1016/j.jmrt.2023. 12.175.
- [20] F. Aydın, K.M. Karaoğlan, H. Y. Pektürk, B. Demir, V. Karakurt, and H. Ahlatçı, The comparative evaluation of the wear behavior of epoxy matrix hybrid nanocomposites via experiments and machine learning models. Tribology International, 204, 110451, 2025. https://doi.org/10.1016/j.triboint.2024.110451.

